

Ground-penetrating Radar Clutter Removal via 1D Fast Subband Decomposition

Deniz Kumlu^{#,*}, Gökhan Karasakal[#], Nur Hüseyin Kaplan[@], and Isin Erer[#]

[#]*Department of Electronics and Communications Engineering, Istanbul Technical University, Istanbul - 34469, Turkey*

[@]*Department of Electrical and Electronics Engineering, Erzurum Technical University, Erzurum - 25700, Turkey*

^{*}*E-mail: kumlud@itu.edu.tr*

ABSTRACT

Target detection performance in ground-penetrating radar (GPR) deteriorates highly in the presence of clutter. Multi-scale (wavelet transform) or the recently proposed multi-scale and multi-directional decomposition based methods can efficiently remove the clutter, however they have high computational complexity. In this paper, we propose a new multi-scale method which requires only 1D fast subband decomposition of the rows of the GPR image. The resulting detail layers directly provide the clutter-free target component of the GPR image. The proposed method is compared to the state-of-art clutter removal methods both visually and quantitatively using a realistic simulated dataset which is constructed by the gprMax simulation software. The results show that the proposed 1D subband decomposition scheme approximates the classical 2D wavelet decomposition successfully and even presents a performance increase as well as a complexity decrease for fast decomposition methods based on lifting wavelet transform and a trous wavelet transform.

Keywords: Wavelet transform; Subband decomposition; Landmine detection; Signal extraction; Ground-penetrating radar

1. INTRODUCTION

Landmines and various explosives present a serious problem for many countries around the world. According to the records, there are nearly 110 million buried landmines in 70 countries. An estimated number of victims die every year due to landmine explosions globally is around 26,000¹. Thus, landmine and explosive clearance operations have vital importance. For decades, metal detectors were used prominently for anti-personnel landmine detection, proving high detection rates for landmines with metal ingredients. However, contemporary manufacturers have reduced the metal rates in the landmines, causing the detection rate of metal detectors decrease considerably².

With this development in landmine production technology, ground-penetrating radar (GPR) systems have come into use instead of the conventional metal detectors as the prominent detection tool. GPR is especially effective where plastic anti-personnel landmines are concerned. These landmines are buried close to the ground surface because they are pressure activated^{2,3}. Generally, the depth of the buried antipersonnel landmine varies between 2-10 cm, classifying it as a shallowly buried object. This makes its detection challenging due to the presence of clutter composed of direct-wave, ground-bounce, and reflections from other subsurface discontinuities. Direct-wave is the electromagnetic wave directly propagated by transmitter antenna towards the receiver antenna and it is also known as coupling affect. Ground-bounce is the reflection

from the ground surface and it is very strong compared to other reflected signals from the underground. The reflections caused by other deceptive buried objects such as roots, stones, gravel, etc. can be considered as a part of the clutter, however they are weaker compared to the direct-wave and ground-bounce. Moreover, the electrical properties of the soil type and the surface type also affect the detection performance². These reasons are inherent to the clutter and have no specific trend.

To increase the detection rate of the GPR, the clutter signal, which is much stronger compared to that of the target, must be removed. Various clutter removal methods are proposed in the literature⁴⁻¹³ the most popular ones being the subspace-based clutter removal methods^{6,7} such as principal component analysis (PCA)⁶, independent component analysis (ICA)⁶, singular value decomposition (SVD)⁶, and morphological component analysis (MCA)⁸. PCA, ICA and SVD perform matrix decomposition on the GPR image using different constraints. After the decomposition of the GPR image into multiple sub-images, the most dominant component corresponds to the clutter and the remaining sub-images construct the target component⁶. The recently proposed MCA separates the morphological components (clutter and target for GPR image) using dictionaries which are learnt in the pre-processing step and decomposes the GPR image into clutter and target parts by making successive iterations with the pre-learned dictionaries⁸.

There is also another group of methods based on multi-scale/multi-directional decompositions⁹⁻¹³ where they exploit the intrinsic geometrical properties of the target and clutter. However, they are computationally highly complex and not

appropriate for the real-time implementations. Wavelet-based transforms (WT)⁹⁻¹², curvelet transform (CT)⁷, bilateral filter (BF)⁷, neighborhood filter (NF)¹³ based methods constitute the multi-resolution analysis (MRA) group where the first one uses only the three main directions, namely vertical, horizontal and diagonal while the latter employ more. In wavelet-based methods¹¹⁻¹⁴ the rows and columns of GPR image are sequentially filtered by low-pass (LPF) and high-pass wavelet filters (HPF) with the resulting approximation and detail subbands corresponding to the three main directions (horizontal, vertical and diagonal). The clutter component, which has a horizontal structure, is captured in the horizontal subband while the other subbands contain the target component. CT⁷, BF⁷ or NF¹³ based methods provide a multi-resolution /multi-directional decomposition of GPR image by using many number of directional subbands, thus enabling a better localisation of the target component. Although these approaches have better target detection performance and better clutter removal ability, they are also have high complexity compared to subspace-based methods¹³. In this paper, motivated by the fact that clutter has a horizontal structure, we propose to decompose only the rows of the GPR image, thus the depth data. The decomposition process is performed via an undecimated wavelet transform (UWT), also known as stationary wavelet transform (SWT)¹², as well as fast subband decomposition methods such as lifting wavelet transform (LWT)¹⁴ and a trous wavelet transform (ATWT)¹⁵.

LWT¹⁴ uses second generation wavelets and performs decomposition/reconstruction steps via simple arithmetical operations instead of fast Fourier transform (FFT) based convolution operations of the classical WT. ATWT¹⁵ decomposes the input data into an approximation signal called as the residue and a set of detail signals. Unlike the classical WT which requires filtering in the reconstruction step, the reconstructed signal is directly obtained by the summation of the residue with detail signals.

2. 2D WAVELET TRANSFORM BASED CLUTTER REMOVAL IN GPR

The basic working principle of GPR is based on transmitting and receiving high-frequency electromagnetic pulses from its antennas. The obtained information constitutes the GPR image or the B-scan².

The GPR image is represented by a rectangular matrix $X_{i,j}$ with dimensions $M \times N$, ($m = 1, 2, \dots, M$; $n = 1, 2, \dots, N$).

Here m refers to the time index, and n refers to the distance index. In GPR, A-scan is a 1D signal produced by gprMax software for a single location and GPR image (B-scan) is a 2D signal resulting from a concatenation of A-scan signals as shown in Figs. 1(a)-1(c). The horizontal axis of X matrix corresponds to the distance (cm) while the vertical axis represents the time (ns). Each A-Scan consists of target response and impact of the ground reflection (clutter) which is stronger as shown in Fig. 1(a). Since the ground reflection is stronger, it mostly masks the target, especially when the target is close to the ground surface making detection challenging².

It is possible to obtain a MRA decomposition⁹ of the GPR image as given in Fig. 2. The j 'th-level decomposition formula

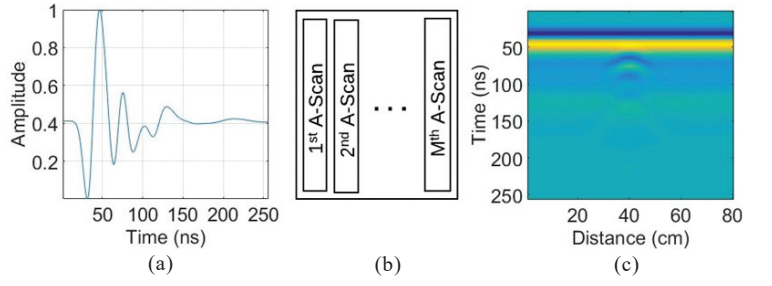


Figure 1. (a) A-scan signal (b) construction of GPR image (c) GPR image (B-scan).

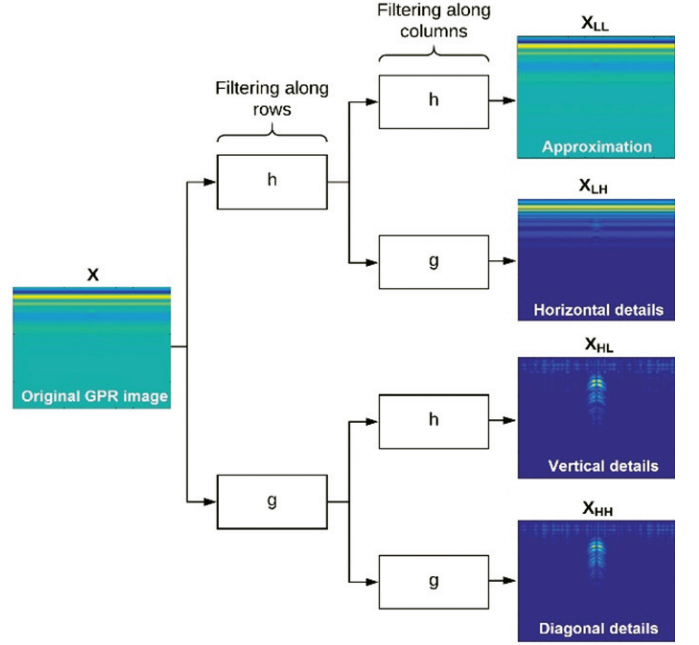


Figure 2. 2 level decomposition of the GPR image by WT.

of the 2D SWT, an undecimated wavelet transform¹², can be given as follows:

$$A_{j,k_1,k_2} = \sum_{n_1} \sum_{n_2} h_0^{\uparrow 2^j} (n_1 - 2k_1) h_0^{\uparrow 2^j} (n_2 - 2k_2) X_{j-1,n_1,n_2}$$

$$D_{j,k_1,k_2}^1 = \sum_{n_1} \sum_{n_2} h_0^{\uparrow 2^j} (n_1 - 2k_1) g_0^{\uparrow 2^j} (n_2 - 2k_2) X_{j-1,n_1,n_2}$$

$$D_{j,k_1,k_2}^2 = \sum_{n_1} \sum_{n_2} g_0^{\uparrow 2^j} (n_1 - 2k_1) h_0^{\uparrow 2^j} (n_2 - 2k_2) X_{j-1,n_1,n_2}$$

$$D_{j,k_1,k_2}^3 = \sum_{n_1} \sum_{n_2} g_0^{\uparrow 2^j} (n_1 - 2k_1) g_0^{\uparrow 2^j} (n_2 - 2k_2) X_{j-1,n_1,n_2}$$

The rows and columns of the input image are filtered sequentially by low pass filter h_0 and high pass 1D filter g_0 where the results A_{j,k_1,k_2} , D_{j,k_1,k_2}^1 , D_{j,k_1,k_2}^2 and D_{j,k_1,k_2}^3 correspond to approximation image X_{LL} and horizontal, vertical and diagonal images X_{LH} , X_{HL} , and X_{HH} respectively.

The clutter has a horizontal structure and it is mainly concentrated in X_{LH} , while the target is represented by the remaining detail images X_{HL} , X_{HH} ⁷. $h_0^{\uparrow 2^j}$, and $g_0^{\uparrow 2^j}$ denote that $2^j - 1$ zeros are inserted between the elements of h_0 , and g_0 . Since the method is based on 2D decomposition of the data, its complexity is high. In the following section, a new clutter removal method which is based only on the 1D subband decomposition of the rows of the GPR image is presented.

3. PROPOSED 1D FAST SUBBAND DECOMPOSITION BASED CLUTTER REMOVAL METHOD

The depth data $x = [x_1, x_2, \dots, x_M]$ corresponding to one row of the GPR image can be decomposed into subbands using 1D MRA similar to the decomposition scheme given in the previous section by filtering the signal with h_0 and g_0 to obtain approximation and detail bands, respectively.

To carry on with the decomposition, approximation band is decomposed to obtain second level approximation and detail subbands. Thus, it is possible to decompose the data signal into an approximation signal (residue) and a set of detail signals as shown in Fig. 3(a).

The procedure can be repeated for all depth signals to give the structure as shown in Fig 3(b). Since this method requires only the decomposition of the rows of the GPR image, its complexity is decreased to the half of the 2D decomposition's. It is possible to decrease the complexity further using faster decomposition approaches such as LWT¹⁴ and ATWT¹⁵. Both methods make use of simple arithmetical operations instead of FFTs, moreover the latter does not require an inverse transform but only the direct summation of detail and approximation subbands to give the reconstructed signal.

3.1 Lifting Wavelet Transform

LWT, also considered as second generation wavelet transform, constitutes of split, predict and update operations for the decimated case¹⁴.

In the split operation, the depth signal x is divided into

$$x_e = x_{2i}, \quad x_o = x_{2i+1} \quad (1)$$

where x_e and x_o denotes even and odd parts.

The odd part is predicted by the even array using a prediction operator $P[\bullet]$. The detail signal d_1 is given as

$$d_1 = x_o - P[x_e] \quad (2)$$

Then low-level signal s_1 is obtained by updating the detail signal d_1 with the update operator $U[\bullet]$ as

$$s_1 = x_e + U[d_1] \quad (3)$$

s_1 is divided again into even and odd array parts and the recursion steps are repeated until $\{s_j, d_j, d_{j-1}, \dots, d_2, d_1\}$ is obtained, where j is the desired stage.

The inverse lifting scheme is straightforward. It is easily obtained by reversing the order of the decomposition steps (update, predict and merge for the inverse transform) and changing “+” to “-” and vice versa. The split step is replaced by

a merge step in the reconstruction. The reconstructed odd and even parts are fused together in each level.

Since the size of the department data must be preserved, it is preferable to adopt the undecimated case. Undecimated LWT consists of only predict and update operations. Instead of the split operation of the decimated case, the prediction and update filters are extended by inserting 2^{j-1} zeros between their samples¹⁴ for each level j as

$$\begin{aligned} P^j &= \{P_0^0, 0, K, 0, P_1^0, 0, K, 0, P_{M-1}^0\} \\ U^j &= \{U_0^0, 0, K, 0, U_1^0, 0, K, 0, U_{N-1}^0\} \\ 0, K, 0 &= 2^{j-1} \text{ number} \end{aligned} \quad (4)$$

here M and N refers the numbers of weight coefficients for filters as given in Eqn. (4).

The reconstruction step involves again reversing of decomposition steps, change of signs and the averaging operation which replaces the merging step¹⁴.

3.2 A Trouis Wavelet Transform

In ATWT, the signal is filtered to obtain the first approximation layer¹⁵.

$$x_1 = x_0 * h_0 \quad (5)$$

where h_0 is the bi-cubic filter given as

$$h_0 = \frac{1}{16} [1 \ 4 \ 6 \ 4 \ 1] \quad (6)$$

here x_0 is the original signal, whereas x_1 is the first approximation layer. The first wavelet layer is simply obtained by

$$W_1 = x - x_1 \quad (7)$$

For further decomposition, the approximation layers have to be filtered again as:

$$x_j = x_{j-1} * h_{j-1} \quad (8)$$

x_j is the approximation layer, while h_{j-1} is the $(j-1)^{th}$ level filter, which is obtained by filling 2^{j-1} zeros between the filter h_0 . The j^{th} level wavelet layer is given by

$$W_j = x_{j-1} - x_j \quad (9)$$

For J levels of decomposition, the original data can be reconstructed as¹⁵

$$x = \sum_{j=1}^J (W_j + x_j) \quad (10)$$

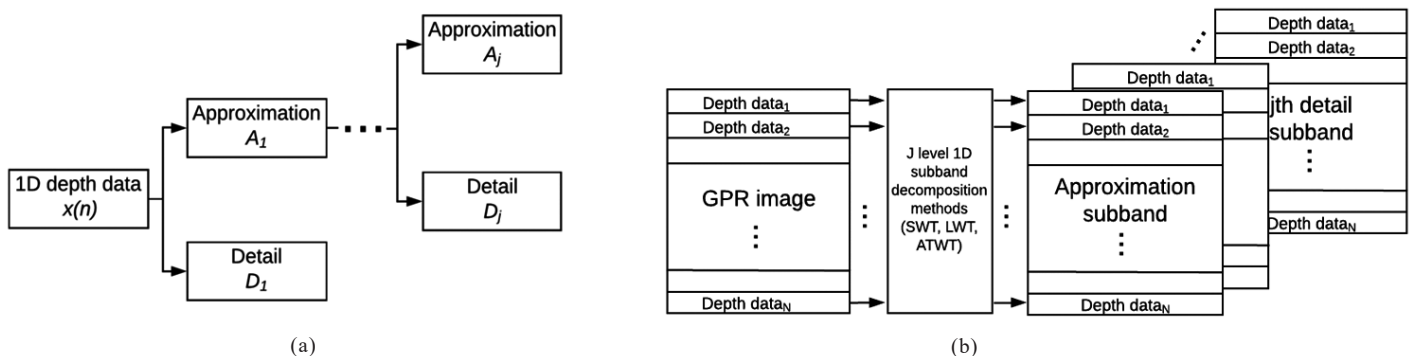


Figure 3. (a) 1D subband decomposition for WT and (b) Implementation in GPR image.

Once the data is decomposed with the methods described above, approximation and the detail subbands are kept and the procedure is repeated for all the rows of GPR image X , as shown in Fig. 3(b). The clutter-free target component is directly provided by the second level detail subband, not requiring any reconstruction step.

4. EXPERIMENTAL RESULTS AND DISCUSSION

The proposed 1D subband decomposition approach based on 1D SWT and the fast approaches based on LWT and ATWT are first compared with 2D SWT¹² using the simulated dataset¹⁶ constructed by gprMax simulation software¹⁷.

In all of the experiments, the commercial antenna is used where it is produced by Geophysical Survey Systems, Inc. (GSSI) (Model 5100) with frequency 1.5 GHz. It is located 5 cm above the surface and moved 1 cm in each iteration. 80 cm area is scanned to construct the GPR image. The constructed simulation dataset contains 112 GPR images with 2 different burial depths (2 cm and 3 cm), 7 different soil types (dry sand, damp sand, wet sand, dry clay soil, wet clay soil, dry loam soil, and heterogeneous soil), 2 different object materials (aluminum, and plastic) and 4 challenging scenarios (flat surface, flat surface with grass, rough surface, and rough surface with water)¹⁶.

The performance comparison is done both quantitatively and visually. The quantitative analysis is carried out by receiver operating characteristics (ROC) curves and area under curve (AUC) which correspond to the area under the ROC curves.

The visual results of the clutter-free GPR image are as shown in Fig. 4(a) and the energy level depends on the pixel intensity values of the clutter-free GPR image. The energy and filtered energy plots are as shown in Fig. 4(b). The initial calculated energy based on pixel intensities is filtered by a low pass filter in order find the trend of energy to obtain more accurate results.

The regions used in the calculation of ROC curves are displayed in Fig. 4(a) (the detection region is between the dotted green line and the false alarm region is outside of the dotted green line). Since a simulated dataset is used, the exact location of the buried object is known. Probability of detection (PD) and false alarm rate (FAR) are obtained with respect to the filtered energy function as shown in Fig. 4(b) and are used to calculate the ROC curves.

Figures 5(a)-5(b) show the quantitative performance

analysis of the simulated dataset (which contains 112 GPR images) without any processing (Raw), and after clutter removal using 2D SWT¹², SWT¹², LWT¹⁴ and ATWT¹⁵. The obtained ROC results in Fig. 5(a) show that 2D SWT is slightly higher than the SWT and LWT. The SWT and LWT have nearly the same performance while LWT is a bit higher. ATWT shows the best performance among them by reaching maximum detection performance with a very low amount of false alarm rate compared to the others. The AUC results in Fig. 5(b) show the performance differences more clearly. One can easily observe that 1D methods can reach the performance of the 2D methods. The fast versions LWT and ATWT outperform 1D SWT based method.

The results of the clutter removal methods for a simulated GPR image of our dataset (2 cm burial depth, dry sand soil type, aluminum material and flat surface scenario) given in the Fig. 1(c) are shown in Figs. 6(a)-6(d). The results of SWT and LWT in Figs. 6(b)-6(c) are similar, however SWT loses more details compared to LWT and the target component seems to spread which is undesired for clutter removal in GPR. 2D SWT

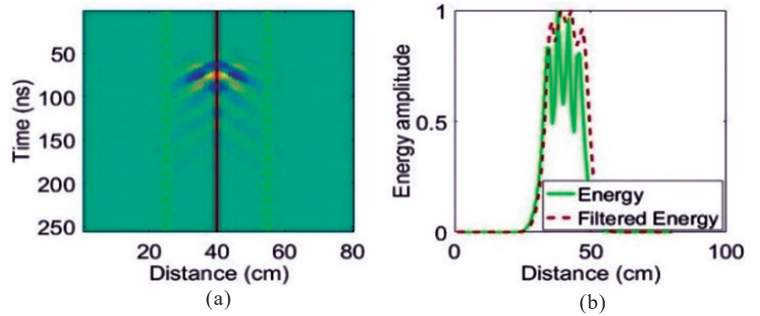


Figure 4. (a) Detection and False alarm regions and (b) Energy and filtered energy plots.

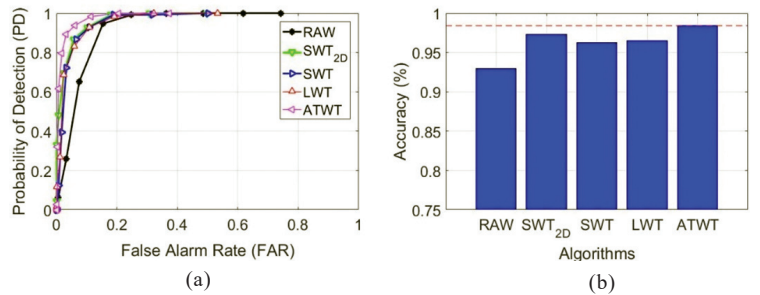


Figure 5. Performance comparisons of the simulated data for 1D subband decomposition methods (a) ROC curves, and (b) AUC.

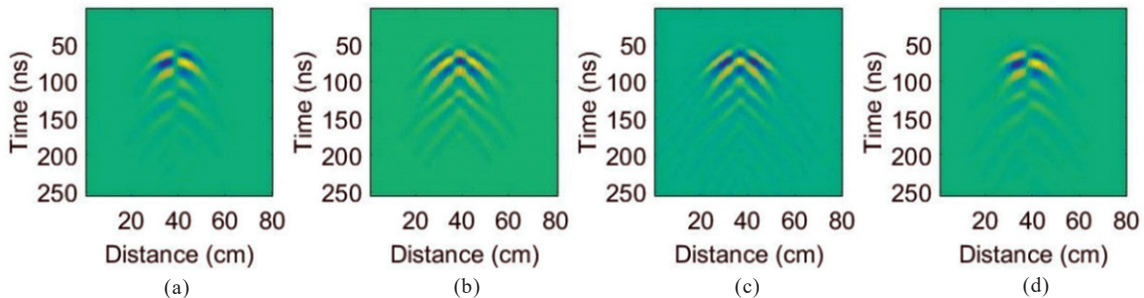


Figure 6. Visual results for GPR image (a) 2D SWT¹² (b) SWT, (c) LWT, (d) ATWT.

result in Fig. 6(a) capture the target component better however the strength of the target signal is weak compared to ATWT. The ATWT result in Fig. 6(d) shows that the method localizes the target component without losing target signal strength. In addition, the background is cleaner compared to the other methods.

Since ATWT outperforms the other 1D subband methods in both quantitative and visual results, we compared it with other state-of-the-art algorithms⁶⁻⁷ such as PCA⁶, ICA⁶, SVD⁶, and MCA⁸. The PCA, ICA and SVD are selected intentionally since they are the fastest clutter removal methods in GPR literature^{6,7}. MCA is not as fast or easily as applicable in real-time application, however it shows best performance among the subspace-based methods⁸.

Figures 7(a)-7(b) show the performance comparison of the methods quantitatively. As seen in the Fig. 7(a), the best performance is obtained by the ATWT method and the second best performance is obtained by MCA. SVD follows them and is slightly below the MCA method. PCA and ICA have comparably lower results than the other methods. Therefore we can conclude that ATWT outperforms all the available fast methods.

From the running times of the methods given in Table 1, it can be observed that MCA has the highest running time among all the compared methods while our proposed 1D fast subband decomposition based methods LWT and ATWT have a running time comparable to SVD and PCA with better performance, thus they are more convenient for real-time applications. The running performance of methods is tested on the Intel core i7 6700HQ @ 2.6GHz, 8GB DDR4-2133, Nvidia GTX950M, on a Windows 10 64-bit environment. Non-optimised codes are used for LWT and ATWT methods.

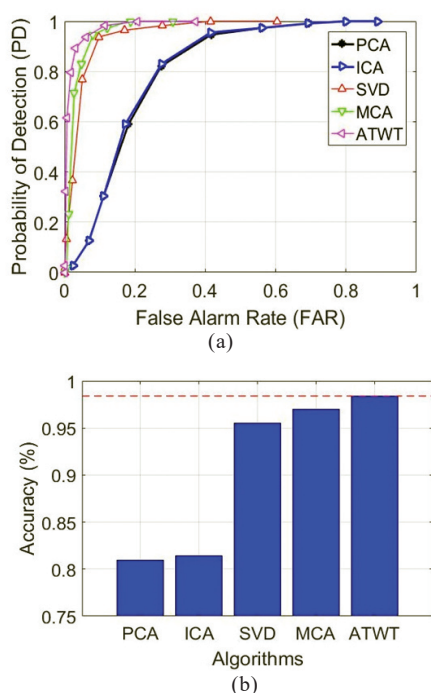


Figure 7. Performance comparisons of the simulated data for ATWT and subspace-based methods (a) ROC curves (b) AUC.

Table 1. Running time of the methods

Methods	PCA	ICA	SVD	MCA	SWT	LWT	ATWT
Time (s)	0.002	0.163	0.004	18.36	0.297	0.024	0.093

5. CONCLUSIONS

A new 1D fast subband decomposition based GPR clutter removal method is proposed. Unlike the SWT based clutter removal method which performs a 2D decomposition of the GPR image, the method requires only 1D decomposition of the rows of the GPR image, performed by 1D SWT or fast methods LWT and ATWT. Thus the complexity is highly reduced making the method competitive with the widely used fast subspace-based clutter removal methods PCA and SVD. The method is validated with visual and quantitative analysis on a realistic simulated dataset provided by the recent version of gprMax simulation tool.

REFERENCES

- Walsh, N. E. & Walsh, W.S. Rehabilitation of landmine victims: the ultimate challenge. *Bull. World Health Organization*, 2003, **81**(9), 665-670.
- Daniels, D.J. Ground penetrating radar. 2nd Ed. Institution of Electrical Engineers, London, U.K., 2004.
- Sinha, A. K. & Mehta, S. D. Detection of landmines. *Def. Sci. J.*, 2001, **51**(2), 115-131. doi: 10.14429/dsj.51.2212
- Kannan O.K.; Bhalla R.; Kapoor J.C.; Nimal A.T.; Mittal U. & Yadava R.D.S. Detection of landmine signature using SAW-based polymer-coated chemical sensor. *Def. Sci. J.*, 2004, **54**(3), 309-315. doi: 10.14429/dsj.54.2044
- Mesecan, I. & Bucak, I. O. Efficient underground object detection for ground penetrating radar signals. *Def. Sci. J.*, 2017, **67**(1), 12-18. doi: 10.14429/dsj.1.9063
- Verma, P.K.; Gaikwad, A.N.; Singh, D. & Nigam, M.J. Analysis of clutter reduction techniques for through wall imaging in UWB range. *Progress In Electromagnetics Research*, 2009, **17**(17), 29-48. doi: 10.2528/PIERB09060903
- Kumlu, D. & Erer, I. Clutter removal techniques in ground penetrating radar for landmine detection: A Survey. *In Operations Research for Military Organizations*, IGI Global, 2019, 375-399. doi: 10.4018/978-1-5225-5513-1.ch016
- Temlioglu, E. & Erer, I. Clutter removal in ground-penetrating radar images using morphological component analysis. *IEEE Geosci. Remote Sensing Lett.*, 2016, **13**(12), 1802-1806. doi: 10.1109/LGRS.2016.2612582
- Carevic, D. Clutter reduction and target detection in ground penetrating radar data using wavelets. *In Proc. SPIE Conference Detection Remediation Technology Mines Mine like Targets IV*, Orlando, FL, 1999, **3710**, 973-979. doi: 10.1117/12.357117
- Zoubir, A. M.; Chant I. J.; Brown, C. L.; Barkat, B. & Abeynayake, C. Signal processing techniques for landmine

- detection using impulse ground penetrating radar. *IEEE Sensors J.*, 2002, **2**(1), 41-51.
doi: 10.1109/7361.987060
11. Ni, S. H.; Huang, Y. H.; Lo, K.F. & Lin, D.C. Buried pipe detection by ground penetrating radar using the discrete wavelet transform. *J. Comput. Geotechnics*, 2010, **37**(4), 440-448.
doi: 10.1016/j.compgeo.2010.01.003
 12. Ben Said, S.; Marzouk, S. B.; Duflos, E.; Vanheeghe, P. & Ellouze, N. Landmines ground-penetrating radar signal enhancement by stationary wavelet transform. *In 12th IFAC Symposium on Large Scale Systems: Theory and Applications*, 2010, **43**(8), 337-340.
doi: 10.3182/20100712-3-FR-2020.00057
 13. Kumlu, D. & Erer, I. The multiscale directional neighborhood filter and its application to clutter removal in GPR data. *Signal, Image Video Process.* 2018, **12**(7), 1237-1244.
doi: 10.1007/s11760-018-1275-z
 14. Sweldens, W. The lifting scheme: A construction of second generation wavelets. *SIAM J. Mathematical Anal.*, 1998, **29**(2), 511-546.
doi: 10.1137/S0036141095289051
 15. Dutilleul, P. An implementation of the 'algorithme à trous' to compute the wavelet transform. *In Wavelets*, Springer, Berlin, Heidelberg, 1990. pp. 298-304.
doi: 10.1007/978-3-642-75988-8_29
 16. Temliolu, E.; Erer, I. & Kumlu, D. A least mean square approach to buried object detection for ground penetrating radar. *In IEEE International Geoscience Remote Sensing Symposium*, 2017, 4833-4836.
doi: 10.1109/IGARSS.2017.8128084
 17. Giannakis, I.; Giannopoulos, A. & Warren, C. A realistic FDTD numerical modeling framework of ground penetrating radar for landmine detection. *IEEE J. Selected Topics Appl. Earth Obser. Remote Sens.*, 2016, **9**(1), 37-51.
doi: 10.1109/JSTARS.2015.2468597

CONTRIBUTORS

Dr Deniz Kumlu received PhD the Department of Electronics and Communication Engineering, Istanbul Technical University, Turkey, in 2018. He is currently working as an instructor at National Defense University/Naval Academy in Istanbul, Turkey. His research interests include remote sensing, image and statistical signal processing.

His contribution to the presented work is to compare the performance of the proposed method with the state-of-the-arts methods.

Mr Gökhan Karasakal is an R&D Engineer at Netas Telecom. A.S., Istanbul, Turkey currently working on his PhD in Istanbul Technical University. His primary research interest include digital signal and image processing.

His contribution to the presented work is to develop codes for fast subband decomposition based clutter removal methods.

Dr N. Hüseyin Kaplan is an Assistant Professor at Electrical and Electronics Engineering Department, Erzurum, Turkey who received his PhD in Electronics and Telecommunication Engineering from Istanbul Technical University, Turkey. His primary research interests include digital signal and image processing

His contribution to the presented work is to provide background about fast subband decomposition methods.

Dr Isin Erer is an Associate Professor in the Department of Electronics and Communication Engineering, Istanbul Technical University, Istanbul, Turkey. Her research interests include: Statistical signal processing, image processing for remote sensing, high-resolution radar imaging and ground penetrating radar. Her contribution to the presented work is to provide overall guidance to the team and combine fast subband decomposition with clutter removal problem.